Journal of
Synchrotron
Radiation

ISSN 0909-0495

Received 9 January 2007
Accepted 23 January 2007

Computed tomography imaging of the neuronal structure of *Drosophila* brain

Ryuta Mizutani,[a]* Akihisa Takeuchi,[b] Tomohiro Hara,[a] Kentaro Uesugi[b] and Yoshio Suzuki[b]

[a]Department of Applied Biochemistry, School of Engineering, Tokai University, 1117 Kitakaname, Hiratsuka, Kanagawa 259-1292, Japan, and [b]Life and Environmental Division, JASRI/SPring-8, 1-1-1 Kouto, Sayo, Hyogo 679-5198, Japan. E-mail: ryuta@keyaki.cc.u-tokai.ac.jp

The neural circuit of the central nervous system (CNS) primarily determines brain functions and, as a consequence, controls animal behavior. This paper describes an X-ray microtomographic analysis of the *Drosophila* larvae CNS, visualizing the neural network embedded in the three-dimensional structure of the nerve tissue. In fluorescence confocal microscopy, absorbance at emission or excitation wavelengths interferes with the fluorescence detection. In contrast, transparency of the nerve tissue to hard X-rays enables tomographic analysis of the intact CNS without sectioning. Yet the nerve tissue is composed of light elements that give little contrast in a hard X-ray transmission image. The contrast was enhanced by staining neuropils in the CNS with metal elements. The obtained structure revealed the internal architecture of the CNS. This metal-staining microtomographic analysis can be applied to any nerve tissues, thereby shedding light on the underlying structural basis of neural functions.

© 2007 International Union of Crystallography
Printed in Singapore – all rights reserved

Keywords: microtomography; impregnation; microcontrasting; neuron; central nervous system.

1. Introduction

Three-dimensional structures of biological molecules determine the molecular mechanism of biological functions; however, little is known about the higher-order three-dimensional structures of biological systems including nerve tissue. Confocal optical-microscopy is the primary method for illustrating three-dimensional structures of the higher-order systems (Conchello & Lichtman, 2005). Since structures within opaque scaffolds are impossible to access by optical microscopy, universally stained tissues are subjected to microtomy procedures. Even in rather transparent tissues, image quality deteriorates at greater depth in the three-dimensional image. Therefore, elaborations are needed to attain high-resolution deep imaging (Hashimoto *et al.*, 1999; Zhang *et al.*, 2006). Although the maximum spatial resolution of an optical microscope is estimated to be about half the observation wavelength (200–300 nm), the observation depth is typically limited to 100 μm in confocal microscopy. This causes difficulties in three-dimensional reconstruction of the entire optical image of thick samples.

In the central nervous system (CNS), a great number of neurons comprise complicated neural networks, making it difficult to dissect the connectivity of each neuron. These neurons consist of cell bodies (typical diameter 10–30 μm), dendrite segments (0.3–1.0 μm) and axons (1–3 μm). The neurons are connected by a characteristic structure called a synapse, in which neural transmitters mediate nerve excitement through the synaptic gap (~20 nm). In order to visualize the neuronal architecture of the CNS by optical microscopy, nerve tissue is stained with selective probes so as to confine observation of projection patterns to a specific neuron. Reconstruction of the entire three-dimensional structure from such optical images of individual neurons entails defining the precise spatial relationships of each image. However, individual variations in size, shape and proportion of the CNS structure of each preparation raise constitutive difficulties in superposing multiple images.

X-ray computed tomography (CT) is a widely used technique for imaging three-dimensional internal structures. Recent application of synchrotron radiation to high-resolution CT (micro-CT) has resolved three-dimensional structures at micrometer (Uesugi *et al.*, 2001) to submicrometer scales (Takeuchi *et al.*, 2002). Micro-CT analysis is generally used for objects containing metal elements because they give an appropriate contrast even in hard X-ray regions. Its application to biological materials is problematic because they are composed of lighter elements. The contrast can be enhanced by using soft X-rays, which are effectively absorbed by biological materials (Watanabe & Aoki, 1998), or by applying the phase-contrast technique to develop the interferometric images (Momose *et al.*, 1996). However, the application of

these methods is limited to samples through which soft X-rays can pass or that give an inherent contrast in a phase-shift cross section.

A number of methods can be used for staining biological tissues with fluorescent and pigment probes. Labeling of the target tissue with an electron-dense probe facilitates acquiring contrasty X-ray images of biological objects. The neuropil features in the CNS can be microscopically observed by impregnating them with silver and gold (Heinz, 2005). The entire structure of the nerve tissue in the CNS can therefore be visualized by the use of metal impregnation and CT analysis (Mizutani *et al.*, 2006). Here we report an X-ray microtomographic analysis of the metal-stained *Drosophila* CNS.

2. Materials and methods

2.1. *Drosophila* CNS

We used the CNSs of *Drosophila* larvae for three-dimensional structure analysis since the sample size is limited to less than about 1.0 mm with the present micro-CT set-up. Wild-type *D. melanogaster* Canton-S larvae were raised on standard cornmeal-molasses fly food and kept at 298 K. The CNSs of third instar larvae were dissected and fixed for 30 min in a solution containing 85% ethanol, 5% acetic acid and 4% formaldehyde. After being washed with 95% ethanol, the CNSs were progressively hydrated in 90%, 70%, 50% and 30% ethanol and then in distilled water. These rehydrated CNSs were subjected to modified reduced-silver staining (Heisenberg, 1989), which reveals neurofilaments in every neuron (Tyrer *et al.*, 2000). The impregnation was performed for 15 h at 310 K using 0.04% silver nitrate solution containing 0.75% pyridine and 25 m*M* sodium borate (pH 8.4). The CNS samples were then developed for 10 min at 298 K in a solution containing 1% hydroquinone and 10% sodium sulfite. After being washed with distilled water twice, the samples were immersed sequentially in 1% hydrogen tetrachloroaurate for 20 min, 2% oxalic acid for 10 min and 5% sodium thiosulfate for 5 min, with a 4 min wash in distilled water between immersions. After removal of the residual sodium thiosulfate by washing, the samples were dehydrated in an ethanol series and transferred to xylene. For tomographic analysis, the samples were mounted on nylon loops like those used in protein cryo-crystallography (Teng, 1990) and then embedded in Petropoxy 154 epoxy resin (Burnham Petrographics, ID, USA).

2.2. Scanning electron microscopy

Scanning-electron-microscopic analysis was performed using a Hitachi S-3200N scanning electron microscope operating at 20 kV. X-ray emission spectra for each CNS area were recorded for 150 s while the backscattered electron images were being observed. The energy resolution was 0.15 keV.

2.3. Micro-CT

Projection-CT analysis was performed using the BL20XU beamline of SPring-8, Harima, Japan. Transmission radiographs were recorded using a CCD-based X-ray imaging detector (AA50 and C4880-41S, Hamamatsu Photonics KK) and 12 keV monochromatic X-rays. The X-ray flux density was estimated to be 4.0×10^{12} photons s^{-1} mm^{-2}. The field of view and effective pixel size of the image detector are 0.94 mm × 0.61 mm and 0.47 µm × 0.47 µm, respectively. Each image was acquired with a rotation step of 0.12° and an exposure time of 300 ms. The convolution back-projection method using a Chesler-type filter was used for tomographic reconstruction (Uesugi *et al.*, 2001). X-ray absorption fine structure (XAFS) spectra were also recorded using the BL20XU beamline. Volume-rendered figures of the obtained three-dimensional structures were produced using the *VG Studio MAX* software (Volume Graphics GmbH, Germany).

Higher-resolution X-ray transmit images were obtained using an X-ray microscope optics at the BL47XU beamline of SPring-8 (Uesugi *et al.*, 2006). A Fresnel zone plate was adopted as an X-ray objective lens in this optics, achieving a spatial resolution of 160 nm. Two-dimensional radiographs produced by 7.13 keV X-rays were recorded using the CCD-based detector.

The data acquisition conditions are summarized in Table 1.

Table 1
Data acquisition conditions.

	Projection CT	Zone plate microscopy
Beamline	BL20XU	BL47XU
X-ray energy (keV)	12.000	7.130
Pixel size (nm)	474	35
Spatial resolution (nm)	1000	160
ADC bit	12	12
Exposure/frame (s)	0.3	3.0
Total data acquisition time (s)	1800	–

3. Results

3.1. Metal staining

The reduced-silver staining technique is the traditional method used for the optical observation of neuropils. Fig. 1(*a*) shows an optical image of a stained CNS. In the staining procedure, *Drosophila* CNSs treated with silver nitrate followed by hydroquinone gave a black appearance, indicating that silver particles were deposited in the CNS tissue. The CNSs were further toned blue–black by the tetrachloroaurate treatment.

The X-ray emission spectra were recorded for each area of a CNS stained with silver and aurate while the area was observed with a scanning electron microscope. Fig. 1(*b*) shows an example X-ray emission spectrum from a 40 µm × 40 µm area of a supraesophageal ganglion. The emission peaks for every area corresponded to those of the aurate stain dye, indicating that the CNS was uniformly stained by the aurate compound. No emission peak corresponding to silver was observed, which was expected as the silver deposits were replaced with the aurate compound by this method.

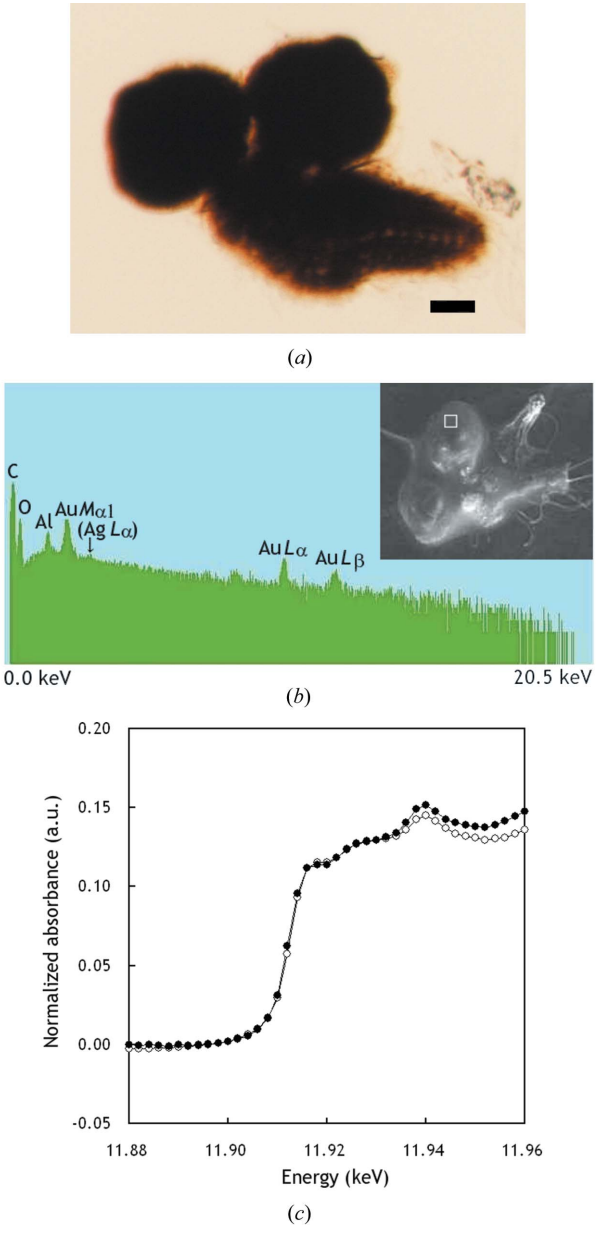

Figure 1
Reduced-silver staining of *Drosophila* larvae CNS. (*a*) Optical microscope image. Scale bar: 50 µm. (*b*) Scanning electron microscopic analysis. X-ray emission spectra were obtained for the 40 µm × 40 µm area indicated in the backscattered electron image shown in the upper-right inset. Emission-line energies of relevant elements are labeled. The aluminium line was from the sample support. Images were obtained using a Hitachi S-3200N scanning electron microscope operating at 20 kV. (*c*) XAFS spectra of the Au L_{III} absorption edge. Closed circles: CNS sample; open circles: 20 µm gold-foil standard.

3.2. CT analysis

Further X-ray spectroscopic and micro-CT analyses were performed at BL20XU of SPring-8 (Uesugi *et al.*, 2001). Results of XAFS spectroscopy revealed that the CNSs contained gold metal particles and not the aurate ions (Fig. 1*c*). The average filling ratio of the gold (estimated from the X-ray extinction coefficient at 12 keV) was 0.24% (*v*/*v*). CNSs exhibiting a higher filling ratio, resulting from an impregnation time longer than the present protocol, showed ambiguous transmission images. This suggests that the filling ratio is a straightforward factor in selecting CNS samples appropriate for micro-CT analysis. It has been reported that optical images are affected by slight changes in the staining protocol (Tyrer *et al.*, 2000).

In the projection tomography, the spatial resolution of the three-dimensional structure was estimated to be 1.0 µm in each direction. The reconstructed images revealed the three-dimensional structure of the CNS, as shown in Fig. 2. The *Drosophila* CNS consists of the right and left brain hemispheres, called supraesophageal ganglions, and the ventral nerve cord. The metal-stained tissue is clearly distinguishable from the epoxy-resin surroundings (Fig. 2*a*), indicating that gold/silver staining can be used for radiographic observation of the CNS.

The image in Fig. 2(*b*) shows a frontal view of the supraesophageal ganglions and ventral nerve cord. The neuropils forming the network are well resolved in the CT image, meaning that the three-dimensional structure can serve as the basis for unraveling the neural circuit. In a stereo rendering of the left supraesophageal ganglion (Fig. 2*c*), the electron-density distribution reveals the overall features of the neural network in the nerve tissue, enabling visualization of the CNS internal structure. The major histological structures of the supraesophageal ganglions are Kenyon cells, the calyx and peduncle of the mushroom body, the dorsal and medial lobes connected to the peduncle, and the optic lobe (Lee *et al.*, 2000; Kurusu *et al.*, 2002; Masuda-Nakagawa *et al.*, 2005). The mushroom body serves as a memory body in insects, and the optic lobe processes visual information in adult insects. In the three-dimensional structure of the supraesophageal ganglion (Fig. 2*c*), Kenyon cells and the calyx of the mushroom body were found in the dorsal cortex. The peduncle of the mushroom body was found to be exserted from the calyx. Axons in the peduncle projected medially and branched into two major lobes, which were assigned to the electron-dense regions of the dorsal and medial lobes. The optic lobe showed a funnel-like structure in the lateral half of the ganglion. A repeated array of electron-dense tubercles was evident in the thoracic and abdominal cortex of the ventral nerve cord. These metal-stained CT images gave a complete view of the *Drosophila* CNS.

It has been estimated that the *Drosophila* larvae CNS consists of about 10000–15000 neurons (Scott *et al.*, 2001). In each CT section, approximately three to five neuropil tracts were observed in a 100 µm^2 area of a 0.47 µm slice. Assuming the volume of the *Drosophila* CNS to be 2×10^7 µm^3, a total of 1.3–2.0 $\times 10^6$ tracts were observed for all the CT sections. Therefore, one neuron should encompass over 100–200 CT sections on average.

3.3. High-resolution radiograph

The higher-resolution images (Fig. 3) were acquired by X-ray microscopy at BL47XU. Fibrilliform structures along with grainy particles were observed in the supraesophageal ganglion (Fig. 3*b*), presumably representing neuronal cell

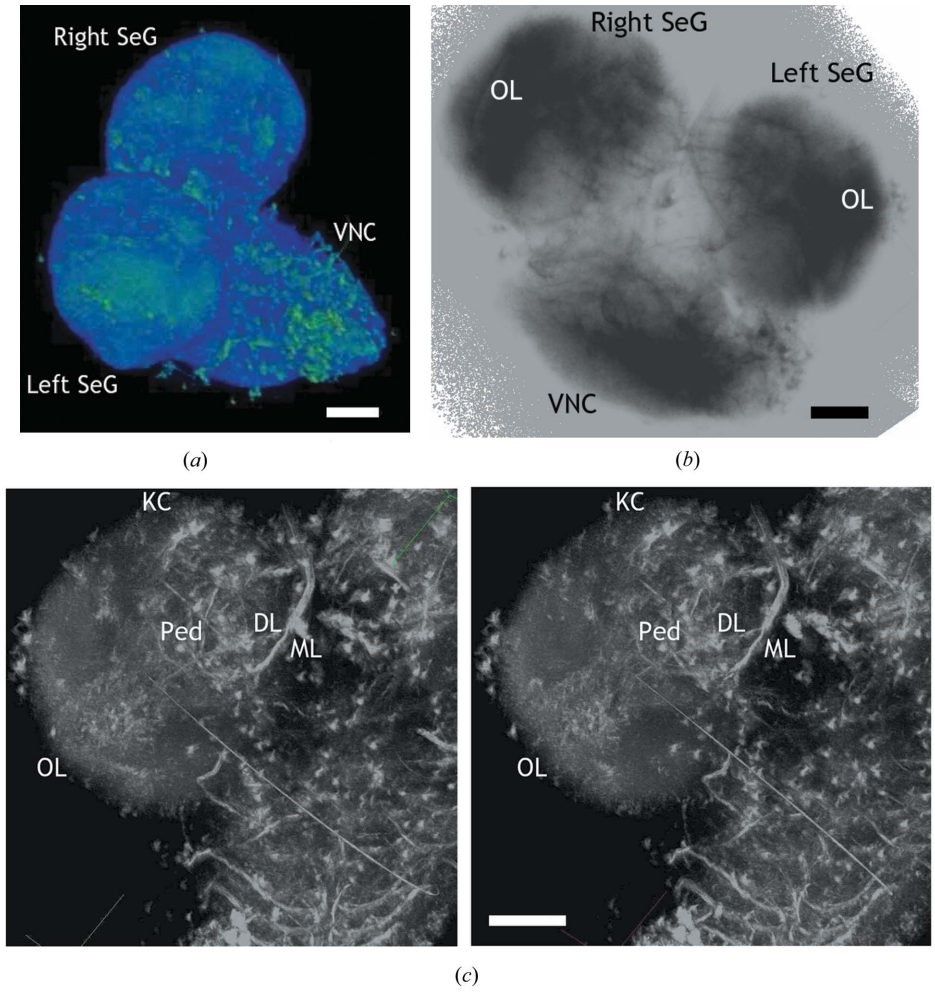

Figure 2
Microtomographic images of CNS. (*a*) Overall image (dorsal view), showing right and left supraesophageal ganglions and ventral nerve cord. Electron densities are colored from the background level (black, corresponding to a linear absorption coefficient of less than 5 cm^{-1}), to low level (blue, 10 cm^{-1}), to high level (green, 35 cm^{-1}). (*b*) Frontal view of the three-dimensional structure. The dorsal is to the top. CT densities were rendered by integrating the absorption of each voxel using *VG Studio MAX* software. (*c*) Stereoview around the left supraesophageal ganglion showing internal neural structure. The sharp arc was noise from the reconstruction calculation. CT densities were rendered using the maximum intensity projection method. Transmission radiographs for CT analysis were recorded using 12 keV X-rays. SeG: supraesophageal ganglion; VNC: ventral nerve cord; Ped: peduncle of the mushroom body; DL: dorsal lobe; ML: medial lobe; OL: optic lobe; KC: Kenyon cells and calyx. Scale bars: 50 µm.

bodies, axons and dendrites comprising the neural network. In the ventral nerve cord (Fig. 3*c*), neurons located in the vicinity of the connective axons running along the cephalocaudal axis are clearly resolved, illustrating the neural circuit that governs the peripheral organs.

4. Discussion

Microscopic structures of biological tissues are generally characterized from thin histological slices. The mechanical stress introduced by microtomy procedures results in physical distortion of the tissue structure, making it difficult to reconstruct the three-dimensional structure from slice images. Fluorescence confocal microscopy is the preferred technique for imaging biological tissues because three-dimensional reconstruction is readily achieved by stacking optical sections. However, absorbance at emission or excitation wavelengths interferes with the detection of fluorescence elicited from the internal architecture. Therefore, confocal microscopy is less successful when many features are stained and is thus primarily used for imaging confined structures labeled with selective-staining probes.

In contrast, the transparency of biological tissue to hard X-rays enables three-dimensional CT analysis of the entire structure. Although the nerve tissue is composed of light elements, which produce little contrast in a hard X-ray transmission image, our results show that the contrast can be enhanced by staining the neuropils with gold particles. The major advantages of such microcontrasting CT analysis with respect to traditional histology are the three-dimensional character of the obtained data and the exclusion of the artificial deformation originating from sectioning or flattened preparation. The three-dimensional architecture of the CNS visualized in this study is comprised of a great number of neurons, which are responsible for the cerebral function. Although the synaptic structure should be further visualized

using electron microscopy techniques, the resolution achieved by the present CT analysis reveals the three-dimensional metal distribution essential for analyzing neuronal networks. Therefore, the functional mechanism of the brain can be revealed by tracing the connectivity of each neuron embedded in the three-dimensional structure. Reconstruction of the three-dimensional structure from the 160 nm resolution radiographs would clarify the precise neuronal structure.

Drosophila CNS is small enough for the present micro-CT experiment set-up. Larger mammalian CNSs are more interesting objects for the elucidation of the entire neural circuit. In simple projection CT geometry, the size limitation due to the experiment set-up can be overcome by modifying the detector face to cover a larger sample area. X-ray transmission scanning pixel by pixel is another strategy for obtaining CT images over a larger field of view, whereas using two-dimensional scanning to acquire transmission radiographs takes much longer. Since the metal impregnation method can be used for any type of nerve tissue, micro-CT analysis with a larger field of view would enable visualization of human cerebral circuits, which are the basis of higher brain functions. Even with the present set-up, a 1 mm^3 block of mammalian nerve tissue, containing 10^3–10^4 neurons, can be visualized as a three-dimensional structure.

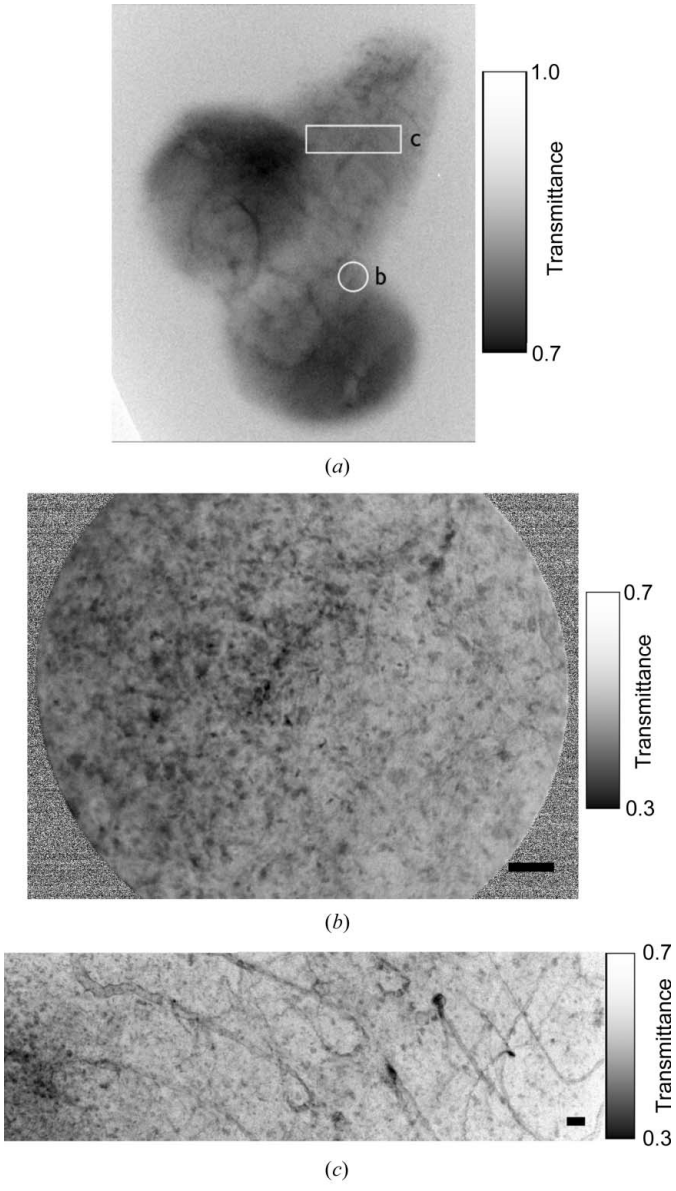

Figure 3
High-resolution radiographs of CNS. (*a*) Overall radiograph taken by projection-CT geometry using 12 keV X-rays. The areas indicated by the circle and rectangle were further radiographed with an objective lens using 7.13 keV X-rays; high-resolution images are shown in (*b*) and (*c*). (*b*) Radiograph of supraesophageal ganglion showing neurons forming elaborate networks. (*c*) Radiograph of ventral nerve cord showing neurons located near connective axons. Transmittances are shown in grayscale. Scale bars: 5 µm.

Selective staining using antibodies and their conjugates has been reported for histological analysis of nerve tissues. Gold and other metal/antibody conjugates used as specific markers, especially in electron microscopic imaging (Zuber *et al.*, 2005), can be applied to the present CT analysis. Ferritin conjugates (Heitzmann & Richards, 1974) are also possible labels for CT observation. Transgenic techniques can be used to locate a certain fluorescent or antigen molecule at a specific site, thereby facilitating development of the CT images. Selective staining of neuronal molecules would enable visualization of the characteristics of the neural connections in the CNS, thereby enabling functional analysis of the neural circuit from the three-dimensional microstructure of the nerve tissue.

Multiple labeling with fluorescent probes has been widely used in confocal microscopic studies (Conchello & Lichtman, 2005). Localization of a probe is determined from its specific fluorescence. Similarly, the distribution of a metal probe can be visualized by observing transmission images at the X-ray absorption edge of the probe element. By applying the selective labeling technique together, we can determine the localization of molecules associated with a particular cerebral function, *e.g.* long-term memory, in the micro-CT image.

Metal staining in conjunction with micro-CT analysis can be applied to any biological system with a three-dimensional structure controlling its functions. Since uniform staining of all the tissue in the structure is essential for visualizing it, a variety of staining methods and dyes should be tested. Along with selective staining, CT analysis can shed light on the underlying microstructural basis of biological functions.

The synchrotron radiation experiments were performed at SPring-8 with the approval of the Japan Synchrotron Radiation Research Institute (JASRI) (Proposal Nos. 2006A1191 and 2006B1716).

References

Conchello, J.-A. & Lichtman, J. W. (2005). *Nature Methods*, **2**, 920–931.
Hashimoto, H., Ishikawa, H. & Kusakabe, M. (1999). *Methods Enzymol.* **307**, 84–107.
Heinz, T. (2005). *Biotech. Histochem.* **80**, 211–222.

Heisenberg, M. (1989). *Drosophila: A Laboratory Manual*, edited by M. Ashburner, pp. 277–278. New York: Cold Spring Harbor Laboratory Press.
Heitzmann, H. & Richards, F. M. (1974). *Proc. Natl. Acad. Sci. USA*, **71**, 3537–3541.
Kurusu, M., Awasaki, T., Masuda-Nakagawa, L. M., Kawauchi, H., Ito, K. & Furukubo-Tokunaga, K. (2002). *Development*, **129**, 409–419.
Lee, T., Marticke, S., Sung, C., Robinow, S. & Luo, L. (2000). *Neuron*, **28**, 807–818.
Masuda-Nakagawa, L. M., Tanaka, N. K. & O'Kane, C. J. (2005). *Proc. Natl. Acad. Sci. USA*, **102**, 19027–19032.
Mizutani, R., Hara, T., Takeuchi, A., Uesugi, K. & Suzuki, Y. (2006). *Proceedings of the Fifth East Asian Biophysics Symposium*, S388.
Momose, A., Takeda, T., Itai, Y. & Hirano, K. (1996). *Nature Med.* **2**, 473–475.
Scott, K., Brady, R. Jr, Cravchik, A., Morozov, P., Rzhetsky, A., Zuker, C. & Axel, R. (2001). *Cell*, **104**, 661–673.
Takeuchi, A., Uesugi, K., Takano, H. & Suzuki, Y. (2002). *Rev. Sci. Instrum.* **73**, 4246–4249.
Teng, T.-Y. (1990). *J. Appl. Cryst.* **23**, 387–391.
Tyrer, N. M., Shepherd, D. & Williams, D. W. (2000). *J. Histochem. Cytochem.* **48**, 1575–1581.
Uesugi, K., Suzuki, Y., Yagi, N., Tsuchiyama, A. & Nakano, T. (2001). *Nucl. Instrum. Methods*, A**467**–**468**, 853–856.
Uesugi, K., Takeuchi, A. & Suzuki, Y. (2006). *Proc. SPIE*, **6318**. In the press.
Watanabe, N. & Aoki, S. (1998). *J. Synchrotron Rad.* **5**, 1088–1089.
Zhang, H. F., Maslov, K., Stoica, G. & Wang, L. V. (2006). *Nature Biotech.* **24**, 848–851.
Zuber, C., Fan, J., Guhl, B. & Roth, J. (2005). *Ultrastruct. Pathol.* **29**, 319–330.